Crystal-induced anisotropy of spin accumulation in Si/MgO/Fe and Si/Al2O3/ferromagnet tunnel devices

Sharma, S.; Spiesser, A.; Saito, H.; Yuasa, S.; van Wees, B. J.; Jansen, R.

Published in:
Physical Review. B: Condensed Matter and Materials Physics

DOI:
10.1103/PhysRevB.87.085307

Publication date:
2013

PHYSICAL REVIEW B **87**, 085307 (2013)

Crystal-induced anisotropy of spin accumulation in Si/MgO/Fe and Si/Al_2O_3/ferromagnet tunnel devices

S. Sharma,[1,2] A. Spiesser,[1] H. Saito,[1] S. Yuasa,[1] B. J. van Wees,[2] and R. Jansen[1]

[1]*National Institute of Advanced Industrial Science and Technology (AIST), Spintronics Research Center, Tsukuba, Ibaraki 305-8568, Japan*

[2]*Zernike Institute for Advanced Materials, Physics of Nanodevices, University of Groningen, 9747 AG, Groningen, The Netherlands*

(Received 20 November 2012; published 13 February 2013)

The effect of crystalline order on the anisotropy of spin accumulation in Si/oxide/ferromagnet tunnel devices has been investigated. The spin accumulation induced electrically in the silicon changes when the magnetization of the ferromagnet is rotated either from *in-plane* to perpendicular to the tunnel interface or when it is rotated within the plane of the magnetic layer. A fourfold *in-plane* anisotropy, which reflects the crystalline nature of the tunnel contact, is observed not only for crystalline MgO/Fe contacts, but also for devices with amorphous Al_2O_3 tunnel barrier and polycrystalline ferromagnetic electrode. The *in-plane* anisotropy is attributed to the direct coupling of states from the ferromagnet to those in the Si, as in coherent tunneling, causing anisotropy in devices in which only the nonmagnetic (Si) electrode is crystalline.

DOI: 10.1103/PhysRevB.87.085307 PACS number(s): 72.25.Hg, 72.25.Dc, 73.40.Gk, 85.75.−d

I. INTRODUCTION

In the field of semiconductor spintronics[1–3] remarkable progress has been made during the past few years, in particular with silicon.[4,5] Magnetic tunnel contacts have emerged as a robust approach to inject and detect spin accumulation in a semiconductor (SC) at room temperature,[6,7] and significant understanding of the physics of spin transport across a magnetic tunnel contact to a semiconductor has been obtained.[4,5] The progress in silicon spintronics has also stimulated research activities with other technologically important semiconductor materials, such as Ge,[8–11] while a variety of oxides (Al_2O_3,[6] SiO_2,[12] and crystalline MgO[8–10,13–15]) have been successfully employed as tunnel barrier in spin tunnel contacts to a SC.

Calculations have predicted very high tunneling magnetoresistance[16,17] (TMR) for crystalline Fe/MgO/Fe magnetic tunnel junctions, and large room temperature TMR has indeed been realized.[18,19] The high tunnel spin polarization (TSP) also makes the crystalline Fe/MgO a system of interest for use in magnetic tunnel contacts to a semiconductor. Besides the large TSP, the crystalline nature of the contacts may also cause anisotropy in the TSP, as found previously for epitaxial (Ga,Mn)As/GaAs contacts.[20] For Si, anisotropy between in-plane and out-of-plane magnetization has recently been reported for devices with an amorphous Al_2O_3 tunnel barrier.[21] However, anisotropy of spin tunneling in MgO-based tunnel contacts to Si has not yet been investigated. Since the anisotropy ultimately arises from spin-orbit interaction, it is of interest to investigate the tunneling anisotropy in silicon devices with crystalline MgO/Fe tunnel contacts.

Here we report the anisotropy of spin accumulation in silicon arising from the anisotropy of spin-polarized tunneling in crystalline Fe/MgO/Si tunnel devices, when the magnetization is rotated either *in plane* or *out of plane*. For out-of-plane rotation of the magnetization, the tunnel resistance does not follow a simple cosine variation, implying that signals of different origin coexist. These tunnel devices also display an in-plane anisotropy with fourfold symmetry that reflects the cubic structure of the crystalline Si/MgO/Fe device. Surprisingly, we also observe in-plane anisotropy in silicon devices with an amorphous Al_2O_3 tunnel barrier and polycrystalline ferromagnet, suggesting a new mechanism of tunneling anisotropy. We attribute it to coherent spin-polarized tunneling across the contact, such that the anisotropy of the tunneling process reflects the cubic symmetry of the crystalline silicon electrode.

This article is organized as follows. Section II describes the sample preparation, structural characterization, and measurement principle. In Sec. III, we first describe the experimental results for *out-of-plane* tunneling anisotropy in crystalline *p*-type Si/MgO/Fe tunnel devices. Then we describe the fitting procedure and discuss the results. This is followed by the data on *in-plane* tunneling anisotropy obtained on magnetic tunnel contacts with a crystalline MgO/Fe contact, and with polycrystalline MgO or an amorphous Al_2O_3 barrier. At the end of this section similar measurements on a control device with zero TSP are shown. A summary is included at the end of the article in Sec. IV.

II. Experiment

A. Device fabrication

The crystalline Fe/MgO tunnel contacts were prepared using the standard fabrication process[6,22] on *p*-type Si wafers with (001) orientation and *B* doping, with carrier density of 4.8×10^{18} cm^{-3} and resistivity of 11 mΩ cm at 300 K. By using wet etching, contact holes were defined through 300 nm of SiO_2, grown at 1150 °C on silicon-on-insulator (SOI) wafers with a 3 μm active Si layer. After etching, the silicon substrates were introduced into an ultrahigh vacuum chamber followed by annealing at 700 °C for 10 min. Subsequently MgO and Fe layers were deposited at 300 °C and 100 °C, respectively. To avoid the oxidation of the magnetic layer, samples were covered by a 20-nm-thick Au capping layer. Subsequently, the ferromagnetic electrode was patterned using Ar-ion milling. This was followed by another lithography step and sputter deposition of Cr/Au contact metals. All the measurements described here have been performed at 300 K on tunnel devices with a contact area of 100×200 μm^2.

The Si/Al_2O_3/ferromagnet tunnel devices were prepared on *n*-type as well as *p*-type SOI wafers. For *n*-type (As-doped)

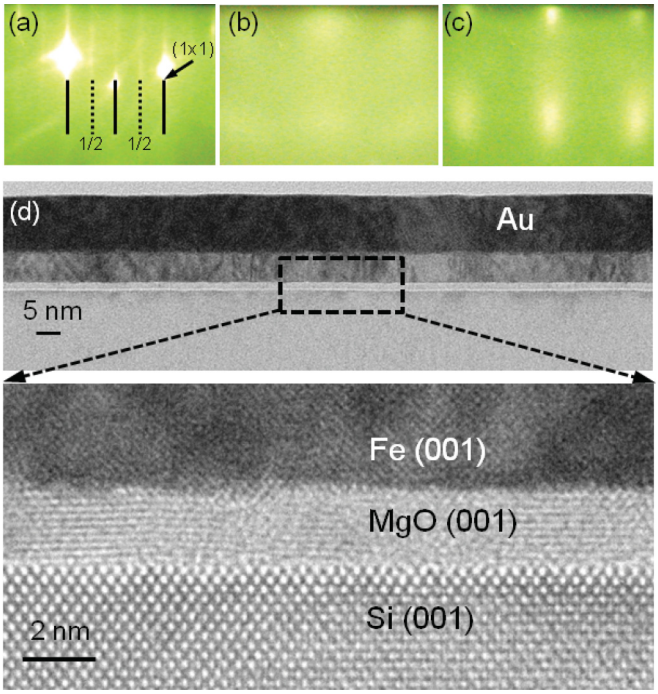

FIG. 1. (Color online) RHEED patterns of (a) the Si surface after annealing at 700 °C, (b) the MgO layer deposited at 300 °C, (c) the Fe layer deposited at 100 °C, and (d) the corresponding high-resolution TEM image of the sample.

Si, with a 5-μm-thick active Si layer, the resistivity and carrier concentration were found to be 3 mΩ cm and 1.8×10^{19} cm^{-3}, respectively, at 300 K. The *p*-type silicon has the same electrical parameters as given above for devices with MgO/Fe tunnel contacts. For making amorphous Al_2O_3/Si contacts, the contact holes of area 100×200 μm^2 were made through SiO_2 by using wet etching. After loading the Si substrate into the ultrahigh vacuum chamber, Al_2O_3 was deposited by electron-beam (*e*-beam) evaporation from a single crystal Al_2O_3 source. A plasma oxidation for 2.5 min was carried out to compensate for the oxygen vacancies known to occur during *e*-beam evaporation of Al_2O_3. This was followed by the *e*-beam deposition of the ferromagnetic layer and the Au cap layer at room temperature. Subsequently, the ferromagnetic electrodes were patterned in a lithography step followed by ion beam etching. Finally, Cr/Au contact layers were deposited by using sputtering.

B. Structural characterization

Structural analysis of the tunnel contacts was performed using *in situ* reflection high-energy electron diffraction (RHEED) and high-resolution transmission electron microscopy (HRTEM). Figure 1(a) shows the RHEED pattern on the Si surface after annealing at 700 °C for 10 min. A Si surface with well-defined (2×1) reconstruction is obtained. The subsequent deposition of MgO on this reconstructed surface results in a spotty pattern [Fig. 1(b)] corresponding to MgO (001). Finally, after deposition of the Fe layer at 100 °C, a spotty RHEED pattern corresponding to crystalline Fe(001) is observed [Fig. 1(c)]. The HRTEM image [Fig. 1(d)] of the sample reveals that smooth and sharp interfaces without interdiffusion and/or intermixing between Si, MgO, and Fe are obtained. A flat interface between Si and MgO with atomic planes in the MgO layer visible indicates an ordered crystalline tunnel barrier. However, at certain locations inside the MgO barrier more disordered or amorphous zones can also be seen. A more detailed analysis reveals the cube-on-cube growth of MgO on Si, whereas the Fe lattice is rotated by 45° with respect to the MgO lattice.[15] These structural characterizations confirm the crystalline nature of the tunnel contacts.

It should be noted that if the annealing of the silicon substrate at 700 °C is omitted, a 1×1 RHEED pattern of the Si surface is obtained. Subsequent MgO and Fe deposition at 300 °C and 100 °C, respectively, results in MgO and Fe layers that are polycrystalline.[15] The anisotropy of these devices has also been studied for comparison. Finally, from previous structural characterization of Si/Al_2O_3/ferromagnet tunnel devices, it is known that the resulting aluminium oxide barrier and the ferromagnetic electrodes are amorphous and polycrystalline, respectively.[23,24]

C. Measurement principle

Two types of anisotropy measurements, namely the field scan and the angle scan, have been performed. In the field scan, the angle ϕ_{out} between the applied field and the surface normal [see Fig. 2(a)] is kept fixed while varying the field strength. The Hanle[6] curve is obtained with the magnetic field perpendicular to the tunnel interface (i.e., $\phi_{\text{out}} = 0°$, 180°, and 360°) and the magnetization lying in the plane of the ferromagnetic layer. On the other hand, with a field parallel to the tunnel interface (i.e., $\phi_{\text{out}} = 90°$ and 270°) and the magnetization still in the plane of the layer, an inverted Hanle curve is obtained.[22] In the second type of measurement, the angle scan, the field strength is fixed at 50 kOe, and the direction of the field is changed by rotating the sample. This rotation can be done in the *out-of-plane* direction (i.e., by varying ϕ_{out}) or in the *in-plane* direction. For the latter, the in-plane field angle ϕ_{in} is defined as the angle between the field (or the magnetization direction) and the (100) crystal axis of the Si electrode [Fig. 2(b)]. For fields of 50 kOe applied in plane, the magnetization is always pointing along the field direction. However, with the applied field out of plane and $0° < \phi_{\text{out}} < 90°$, the magnetization of the magnetic thin film makes a finite angle $\theta = (\phi_M - \phi_{\text{out}})$ with the applied field due to shape anisotropy[21] (see also Sec. III A1). Here, ϕ_M represents the angle between the magnetization direction ($\vec{m}$) and the surface normal [Fig. 2(a)].

In Fig. 2, we depict the measurement geometry using the three-terminal method for spin injection and detection.[6] A constant current I_{bias} results in a voltage $V = V_{\text{Si}} - V_{\text{FM}}$ across the tunnel contact. We adopt the bias convention such that $V < 0$ (or > 0) corresponds to hole injection (extraction) into (from) the valence band of *p*-type silicon. By changing the angle ϕ_{out} (or ϕ_{in}), and applying a fixed bias current I_{bias}, across the tunnel contact, the voltage is $V_{\text{meas}} = V_0 + V_{\text{TAMR}} + V_{\text{ASA}}[\Delta\mu(\phi_{\text{out}},\phi_{\text{in}})]$. The first term on the right-hand side is a constant voltage. The second term (V_{TAMR}) is due to the regular tunneling anisotropic magnetoresistance[2,25–27] (TAMR). This TAMR refers to the change in the tunnel resistance when the magnetization of the magnetic layer is rotated (either within the plane of the magnetic layer or rotated from in plane to out of

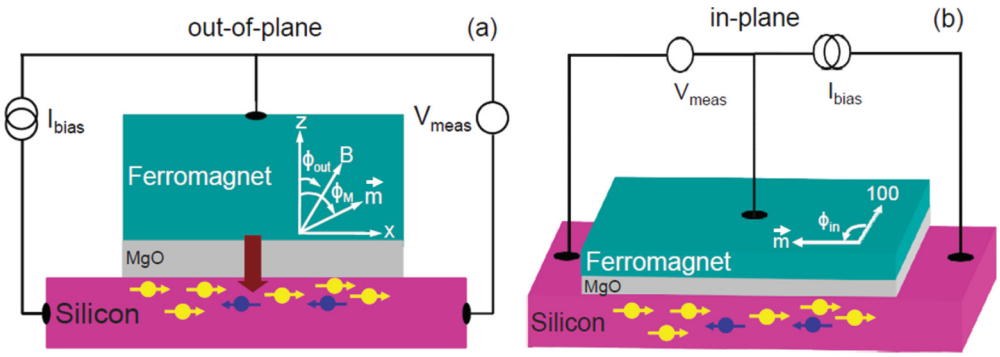

FIG. 2. (Color online) Schematic of the three-terminal technique employed for measuring the (a) out-of-plane and (b) in-plane tunneling anisotropy. A constant current (I_{bias}) across the tunnel contact results in a voltage (V_{meas}) that changes when the magnetization is rotated, either from in plane to out of plane or within the plane of the magnetic layer. In (a), ϕ_{out} represents the angle between the applied magnetic field and the surface normal, while ϕ_M is the angle between the magnetization ($\vec{m}$) and the surface normal directed along the Z axis. The in-plane component of the magnetization lies along X. In (b), ϕ_{in} is the angle between the field (or magnetization) direction and the (100) crystal axis of the silicon.

plane). The anisotropy originates from spin-orbit interaction at the interface between the ferromagnet and the tunnel barrier. The last term $V_{\text{ASA}}[\Delta\mu(\phi_{\text{out}},\phi_{\text{in}})]$ refers to a voltage signal arising from an anisotropic spin accumulation (ASA), i.e., a spin accumulation $\Delta\mu(\phi_{\text{out}},\phi_{\text{in}})$ that depends on ϕ_{out} and/or ϕ_{in}. This can be expected if the tunnel spin polarization of the magnetic contact is anisotropic which leads to a spin accumulation $\Delta\mu$ in the silicon that depends on ϕ_{out} and/or ϕ_{in}. In addition, an anisotropic spin-relaxation time τ_s in the silicon will also result in an anisotropy of $\Delta\mu$.

III. Experimental results

We performed out-of-plane as well as in-plane tunneling anisotropy measurements on magnetic tunnel devices made on p-type silicon with a crystalline MgO/Fe tunnel contact. On the other hand, only in-plane tunneling anisotropy measurements will be shown for tunnel contacts with amorphous Al_2O_3 and a polycrystalline ferromagnetic layer. For the latter case, a detailed study of the out-of-plane tunneling anisotropy has been reported previously.[21]

A. Out-of-plane tunneling anisotropy

Hanle and inverted Hanle measurements are shown in Fig. 3(a) for a spin-tunnel contact with a 2.5-nm-thick MgO as a tunnel barrier. The field scan with the field perpendicular to the tunnel interface results in a symmetric Hanle (red) peak around zero field. By increasing the field, spin precession reduces the signal. A further increase of the field results in an upturn in the signal due to rotation of the magnetization of the ferromagnet towards the out-of-plane direction. Above approximately 22 kOe, when the magnetization has aligned itself with the external field, meaning that there is no more spin precession, the signal settles (it increases only slightly with a linear slope, which is attributed to a background signal). On the other hand, when the applied field is parallel to the tunnel interface, the inverted Hanle curve (blue) is obtained. The inverted Hanle curve exhibits a suppression of the spin signal in the absence of external field due to spin precession in spatially inhomogeneous local magnetostatic fields arising from the finite roughness of the interfaces of the ferromagnetic layer.[22] At a sufficiently large in-plane field, the signal recovers and becomes independent of the external field.

At 50 kOe, irrespective of the field direction, there is no spin precession because the magnetization, external field, and spins injected into the silicon all have the same orientation. Nevertheless, the Hanle and inverted Hanle curves settle at two different levels. As shown in Fig. 3(a), at 50 kOe these curves have a difference of about ≈ 440 μV. This result is reproduced in the angle scan measurement shown in Fig. 3(b) taken with a constant field of 50 kOe. Thus the situations when the field is parallel or perpendicular to the tunnel interface are not equivalent. That is, there is an anisotropy in the measured voltage. It depends on the absolute orientation of the magnetization of the ferromagnetic electrode. Further, the

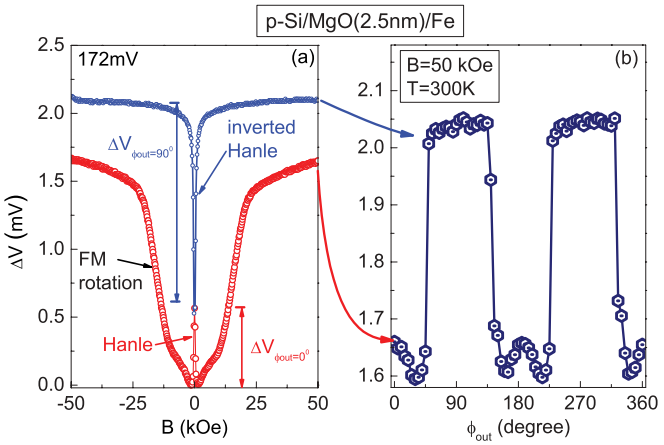

FIG. 3. (Color online) Experimental data for a crystalline p-Si/MgO/Fe tunnel contact with a 2.5-nm-thick MgO barrier. Data are shown with the magnetic field applied (a) perpendicular (Hanle, red) and parallel (inverted Hanle, blue) to the tunnel interface. $\Delta V_{\phi_{\text{out}}=0^\circ}$ and $\Delta V_{\phi_{\text{out}}=90^\circ}$ are the Hanle and inverted Hanle signal amplitudes, respectively. (b) Angular variation of the measured signal (for out-of-plane rotation of the magnetization) at the same bias voltage. Data is shown after subtracting a constant voltage of 172 mV ($I_{\text{bias}} = 39$ μA).

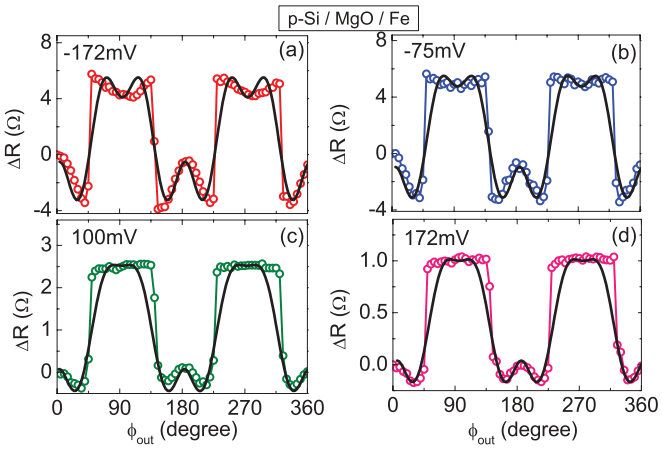

FIG. 4. (Color online) Angular variation of the change in the tunnel resistance $\Delta R = R(\phi_{\rm out}) - R(\phi_{\rm out} = 0^\circ)$, when the magnetization is rotated out of plane at (a) −172 mV, (b) −75 mV, (c) 100 mV, and (d) 172 mV. All data were taken at 300 K and a field of 50 kOe. Solid black lines represent the fits obtained using Eq. (1) described in the text.

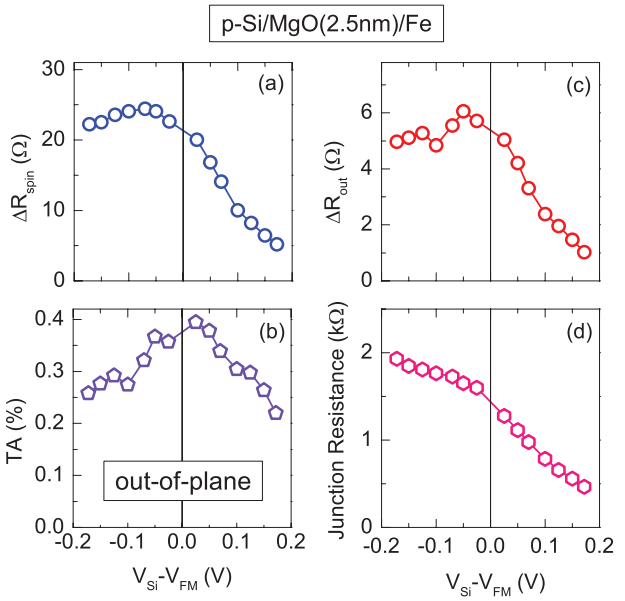

FIG. 5. (Color online) Bias variation of (a) the spin resistance, $\Delta R_{\rm spin} = [\Delta V_{\phi_{\rm out}=0^\circ} + \Delta V_{\phi_{\rm out}=90^\circ}]/I_{\rm bias}$, (b) the out-of-plane tunnel anisotropy percentage (TA), (c) the out-of-plane anisotropy signal $\Delta R_{\rm out} = (R_{\phi_{\rm out}=90^\circ} - R_{\phi_{\rm out}=180^\circ})$, and (d) the junction resistance $(V_{\rm meas}/I_{\rm bias})$ for a *p*-type Si/MgO/Fe tunnel device. Note that $\Delta V_{\phi_{\rm out}=0^\circ}$ and $\Delta V_{\phi_{\rm out}=90^\circ}$ have been defined in Fig. 3(a).

angle scan in Fig. 3(b) shows that the measured voltage has a nonsinusoidal variation with the field angle. This suggests that different contributions to the tunneling anisotropy coexist, as noted previously for tunnel contacts with amorphous Al_2O_3 tunnel barrier.[21]

For the same tunnel device, Fig. 4 shows the bias variation of the change in resistance $\Delta R = R(\phi_{\rm out}) - R(\phi_{\rm out} = 0^\circ)$, where $R(\phi_{\rm out}) = V_{\rm meas}/I_{\rm bias}$ is the resistance at a field angle $\phi_{\rm out}$. The tunnel resistance has four local minima at ≈40°, 160°, 215°, and 340° for all bias voltages. Another two local minima can be seen at ≈90° and ≈270° but only for negative bias voltages. Nevertheless, the overall shape of the signal does not change much with bias voltage.

1. *Analysis and discussion of out-of-plane anisotropy*

For further analysis, we compare the anisotropy with the spin resistance, defined as $\Delta R_{\rm spin} = [\Delta V_{\phi_{\rm out}=0^\circ} + \Delta V_{\phi_{\rm out}=90^\circ}]/I_{\rm bias}$, where $\Delta V_{\phi_{\rm out}=0^\circ}$ and $\Delta V_{\phi_{\rm out}=90^\circ}$ are defined as the Hanle and inverted Hanle signal amplitudes as shown in Fig. 3(a). The quantity $\Delta R_{\rm spin}$ is proportional to the spin accumulation. The bias variation of the spin resistance is shown in Fig. 5(a). As observed earlier,[6,28] the spin resistance is larger for $V < 0$ (hole injection) and decays almost linearly for $V > 0$ (hole extraction). We compare this to the *out-of-plane* anisotropy signal, i.e., $\Delta R_{\rm out} = R_{\phi_{\rm out}=90^\circ} - R_{\phi_{\rm out}=180^\circ}$, shown in Fig. 5(c). It has a bias variation similar to the spin resistance. We also define the *out-of-plane* tunneling anisotropy as $[R(\phi_{\rm out} = 90^\circ) - R(\phi_{\rm out} = 180^\circ)]/R(\phi_{\rm out} = 180^\circ)$. As shown in Fig. 5(b) the tunneling anisotropy decays almost symmetrically with bias voltage. Finally, the regular resistance of the contact versus bias voltage is shown in Fig. 5(d). The junction resistance decreases for positive bias voltage, whereas it is increasing for the negative bias voltages.

Next, we describe the fitting of the experimental data with an equation containing terms arising from an anisotropic spin accumulation, Hanle spin precession, and/or TAMR. As found earlier for devices with Al_2O_3 tunnel barrier,[21,27] the measured tunnel resistance for out-of-plane rotation of the magnetization can be described by an equation that consists of terms with twofold and sixfold symmetry:

$$\Delta R = A_0 + A_1\cos(2\phi_{\rm out}) + A_2\cos(6\phi_{\rm out}) + \Delta R_{\rm spin}\cos^2(\phi_M - \phi_{\rm out}), \quad (1)$$

where A_0 is a constant and A_1 and A_2 are the fitting parameters.[29] The factor $\cos^2(\phi_M - \phi_{\rm out})$ in the last term is due to Hanle spin precession due to the small misalignment between field and magnetization arising from magnetic shape anisotropy of the thin magnetic layer.[21] The magnetic shape anisotropy of a thin (≈20 nm) ferromagnetic film favors a magnetization direction parallel to the surface, i.e., within the film plane, whereas an external field of 50 kOe favors the magnetization to align with it. As a result, the external field and the magnetization are not perfectly aligned, but they make a different angle $\phi_{\rm out}$ and ϕ_M [Fig. 2(a)] with the surface normal, respectively.[21] Due to this misalignment of the magnetization and the external field, the spins injected into silicon make an angle $\theta = \phi_M - \phi_{\rm out}$ with the field, thereby leading to the spin precession in the Si, even at a field of 50 kOe. The net signal due to this effect will be proportional to the spin accumulation, i.e., to $\Delta R_{\rm spin}\cos^2(\phi_M - \phi_{\rm out})$.

The fits to the data using Eq. (1) are shown as solid black lines in Fig. 4. Reasonably good fitting to the data can be achieved by considering terms with twofold and sixfold symmetry. It is found that inclusion of a tenfold term improves the fitting with the data (not shown), but it does not affect the other terms. We therefore limited ourselves to terms up to sixfold symmetry. The fitting parameters A_1 and A_2 for this tunnel contact are shown in Fig. 6. The A_1 is negative, over the full bias range. It is almost constant for $V < 0$ and

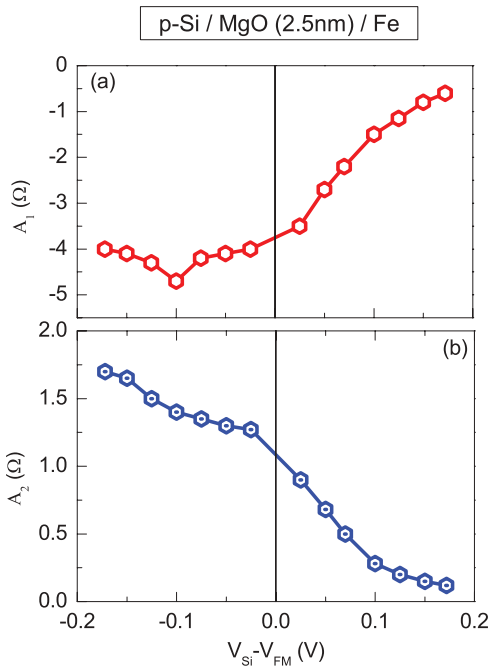

FIG. 6. (Color online) Bias variation of fitting parameters A_1 and A_2 corresponding to the out-of-plane tunneling anisotropy of a p-type Si/MgO/Fe tunnel device.

reduces linearly for $V > 0$. On the other hand, A_2 is positive and decays towards positive bias.

For the interpretation of these results, we will use the following criteria.[21] The spin resistance ΔR_{spin} is proportional to the spin accumulation $\Delta\mu$ in the silicon. Thus, if any of the fitting parameters (i.e., A_1 or A_2) behaves as a function of bias in the same way as ΔR_{spin} does, then we assume that the corresponding anisotropy comes from the anisotropic spin accumulation term $V_{\text{ASA}}[\Delta\mu(\phi_{\text{out}})]$. Both A_1 and A_2 have a bias variation that is similar to ΔR_{spin} and to the junction resistance, although A_1 seems to follow ΔR_{spin} more closely (except for the opposite sign), whereas A_2 follows the tunnel resistance more closely. While the difference is small, this suggests that the term A_1 is dominated by anisotropy of the spin accumulation, whereas A_2 is mostly due to TAMR.

B. In-plane tunneling anisotropy

In-plane tunneling anisotropy refers to the change in the tunneling resistance when the magnetization is rotated within the plane of the magnetic layer. We measure the signal in three-terminal configuration by rotating the sample [i.e., by changing the angle ϕ_{in}; see Fig. 2(b)] in an in-plane field of 50 kOe which is large enough to ensure that the magnetization lies always along the field direction. Devices with crystalline and polycrystalline MgO/Fe tunnel contacts as well as those with an amorphous Al_2O_3 as a tunnel barrier and polycrystalline ferromagnet have been evaluated to investigate the exact source of the in-plane tunneling anisotropy. We begin with magnetic tunnel contacts to p-Si with crystalline MgO barrier.

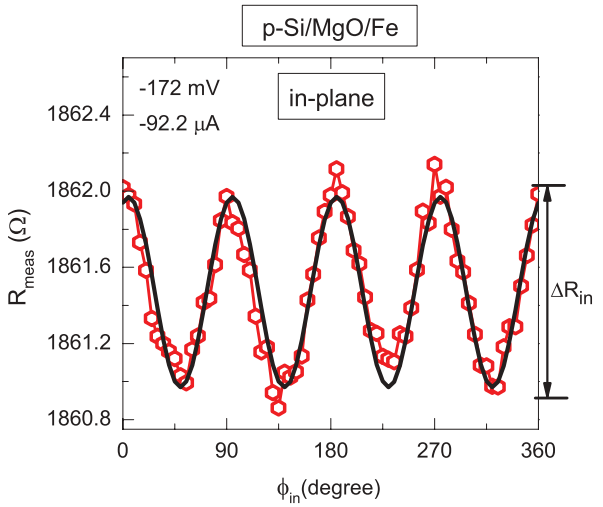

FIG. 7. (Color online) Measured tunnel resistance $R_{\text{meas}} = V_{\text{meas}}/I_{\text{bias}}$ vs angle ϕ_{in} for a p-Si/MgO/Fe tunnel device with 2.5 nm MgO at a bias voltage of -172 mV (-92.2 μA). Here ϕ_{in} refers to the in-plane angle between the magnetization and the (100) crystal axis of the Si electrode [see Fig. 2(b)]. Data was taken at $T = 300$ K.

1. Tunnel contacts with crystalline MgO barrier

A typical measurement on a crystalline MgO/Fe tunnel contact with 2.5 nm MgO is shown in Fig. 7, taken at a bias voltage (current) of -172 mV (-92.2 μA). The tunnel resistance displays an in-plane anisotropy with fourfold symmetry. It has four minima at $\approx 45^\circ$, 135°, 225°, and 315°. We define the in-plane anisotropy signal ΔR_{in} as the maximum peak-to-peak change in tunnel resistance when the magnetization is rotated within the plane of the magnetic layer (see Fig. 7). In Fig. 8(a), the bias variation of the in-plane

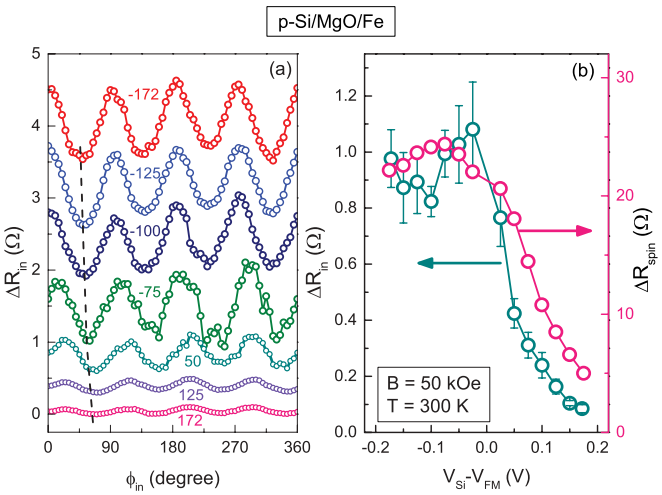

FIG. 8. (Color online) (a) In-plane anisotropy signal (ΔR_{in}) at different bias voltages (in mV) when the magnetization is rotated in the plane of the magnetic layer. Data are displaced vertically for clarity. The black dotted line indicates the shift of the first minima position when the bias voltage is changed from -172 mV to 172 mV. (b) Bias variation of ΔR_{in} shown together with ΔR_{spin}. Note that ΔR_{in} is the peak-to-peak change in tunnel resistance when the magnetization is rotated within the plane of the magnetic layer. All data were taken at 300 K.

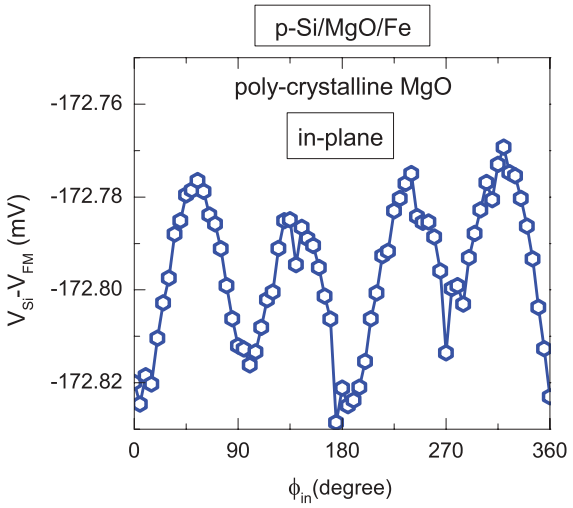

FIG. 9. (Color online) Angular variation in the measured voltage for in-plane rotation of the magnetization for a tunnel device on p-Si with polycrystalline MgO/Fe contact. The measurement was taken with a bias current $I_{bias} = -582\ \mu$A (-172 mV) at 300 K. Note that the vertical scale is the measured (negative) voltage, and that the current is also negative, such that the maximum of resistance occurs at 0°, 90°, 180°, 270°, and 360°, just as in Fig. 7.

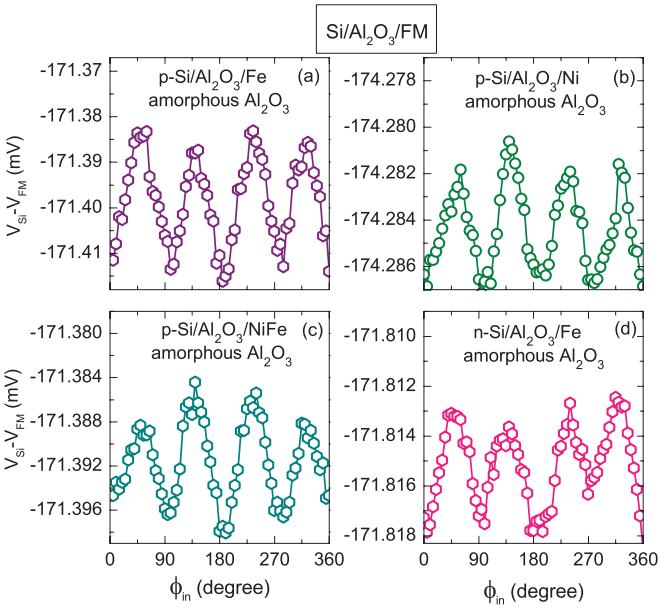

FIG. 10. (Color online) Angular variation in the measured voltage for in-plane rotation of the magnetization for (a) p-Si/Al_2O_3/Fe at $I_{bias} = -97.13\ \mu$A, (b) p-Si/Al_2O_3/Ni at $I_{bias} = -192\ \mu$A, (c) p-Si/Al_2O_3/NiFe at $I_{bias} = -480\ \mu$A, and (d) n-Si/Al_2O_3/Fe at $I_{bias} = -777\ \mu$A. Note that these devices have amorphous Al_2O_3 and polycrystalline ferromagnet. All measurements were taken at 300 K. Note that the vertical scale is the measured (negative) voltage, and that the current is also negative, such that the maximum of resistance occurs at 0°, 90°, 180°, 270°, and 360°, just as in Fig. 7.

anisotropy signal is shown. A fourfold symmetry is obtained at all bias voltages. At -172 mV, the first minimum in resistance occurs at $\approx 45°$. By increasing the bias voltage from -172 mV to 172 mV, the first minimum position gradually shifts from 45° to 70°. The shift in the position of the minima is indicated by a black dotted line in Fig. 8(a). The bias variation of the in-plane anisotropy signal is shown together with the spin resistance ΔR_{spin} in Fig. 8(b). It is found that ΔR_{in} and ΔR_{spin} have the same qualitative variation with bias voltage. For $V < 0$ (hole injection), ΔR_{in} does not vary much, whereas it decays linearly for $V > 0$ (hole extraction).

2. *Tunnel contacts with polycrystalline MgO barrier*

The crystalline quality of the tunnel contacts has been found to influence the magnitude of the spin accumulation created in a semiconductor.[15] Here we examine the effect of crystalline structure of the tunnel contact on the in-plane tunneling anisotropy using a p-Si/MgO/Fe tunnel device with a polycrystalline MgO/Fe tunnel contact. A measurement at a fixed bias current of $-582\ \mu$A (-172 mV) is shown in Fig. 9. We obtain a signal with fourfold symmetry and amplitude $\approx 40\ \mu$V, which is less than the signal ($\approx 100\ \mu$V) obtained for a tunnel device with a crystalline MgO/Fe contact.

3. *Tunnel contacts with amorphous Al_2O_3 barrier*

The observed in-plane tunneling anisotropy may have different origins, e.g., anisotropic tunnel spin polarization of the magnetic contact and/or the anisotropic spin relaxation time τ_s in silicon.[21] In order to investigate the origin of the anisotropy, we also studied devices with an amorphous tunnel barrier and polycrystalline ferromagnet. We performed angle scans on tunnel contacts to p-Si as well as n-Si, which contain a polycrystalline ferromagnet (Fe or Ni or $Ni_{80}Fe_{20}$) and an Al_2O_3 tunnel barrier that is known to be amorphous.[23,24]

Figure 10 displays angle scans for these tunnel devices at -172 mV. For the p-Si/Al_2O_3/Fe device, we observe a fourfold symmetry with $\approx$20–25 μV change in the signal [Fig. 10(a)].

Similar fourfold features are observed for tunnel devices on p-type Si with Al_2O_3 barrier and Ni [Fig. 10(b)] and $Ni_{80}Fe_{20}$ [Fig. 10(c)] as ferromagnetic electrode. However, the change in signal is small: 4–6 μV and 8–10 μV for tunnel devices with Ni and $Ni_{80}Fe_{20}$ electrodes, respectively. Finally, in Fig. 10(d), it is shown that a device with an Al_2O_3/Fe magnetic tunnel contact to n-type Si has the same fourfold symmetry, with a signal amplitude $\approx$ 4–6 μV. For the p-Si/Al_2O_3/Fe tunnel contact, the bias variation of ΔR_{in} is shown together with ΔR_{spin} in Fig. 11. We see that ΔR_{in} and ΔR_{spin} have qualitatively the same variation with bias voltage.

4. *Discussion of in-plane tunneling anisotropy*

In Table I we have collected the relevant parameters, i.e., the in-plane anisotropy signal ΔR_{in}, the tunnel resistance ($R_{tun} = V_{meas}/I_{bias}$), and the spin resistance ΔR_{spin}, obtained on the various tunnel devices at -172 mV. The magnitude of ΔR_{in} depends on the crystalline quality of the tunnel contact as can be seen from the ratios $\Delta R_{in}/R_{tun}$ and $\Delta R_{in}/R_{spin}$ for these devices. The ratios of these parameters are larger for tunnel devices on p-type Si with crystalline MgO/Fe contact and smaller for the devices with an amorphous Al_2O_3 barrier and polycrystalline Fe as a magnetic electrode. An intermediate value is obtained for the device with a polycrystalline MgO/Fe contact. For the other devices on Si with Al_2O_3, the ratio of these parameters changes by a small amount but does not differ

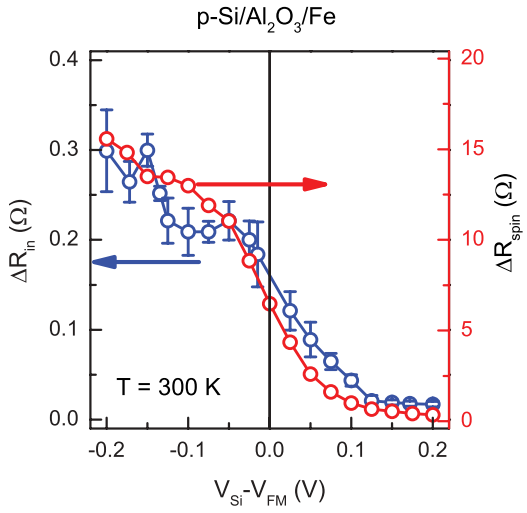

FIG. 11. (Color online) Bias variation of the in-plane anisotropy in tunnel resistance $\Delta R_{\rm in}$ (blue) shown together with the spin resistance (red), i.e., $\Delta R_{\rm spin}$ for a p-type Si/Al_2O_3/Fe tunnel device.

significantly. In crystalline tunnel contacts as well as those with polycrystalline ferromagnet and an amorphous tunnel barrier, the signal $\Delta R_{\rm in}$ due to in-plane anisotropy is a few percent (2% to 5%) of the spin resistance ($\Delta R_{\rm spin}$) and $\Delta R_{\rm in}$ qualitatively has the same bias variation as $\Delta R_{\rm spin}$. This suggests that the observed tunneling anisotropy is due to anisotropic spin accumulation in the silicon.

Although the amplitude of the signal depends on the degree of crystallinity of the tunnel contact, in-plane rotation of the magnetization produces a change in tunnel resistance that has a fourfold symmetry for all the tunnel devices, irrespective of the type of ferromagnet, silicon (n or p type), or crystalline structure of the tunnel contact. For the crystalline p-type Si/MgO/Fe tunnel devices, a fourfold in-plane symmetry is a natural consequence of the cubic crystal structure of the MgO/Fe contact. The crystalline MgO/Fe tunnel contacts on p-type Si display a fourfold symmetry with first minima at 45° at a bias of −172 mV. The minima positions gradually shift to 70° with a change in bias voltage. It is known that in the Fe/MgO system the states with different symmetries have different tunneling probability.[16,17] Their relative contribution may change with bias voltage and this may lead to a change in the position of the minima.

An in-plane TAMR or tunneling anisotropy was not expected in tunnel contacts with amorphous Al_2O_3 tunnel barrier and polycrystalline ferromagnet. However, these contacts also displayed fourfold in-plane symmetry. Below, we discuss the possible sources which may produce the observed in-plane tunneling anisotropy.

(a) An in-plane tunneling anisotropy could arise if the Al_2O_3 tunnel barrier has a crystalline structure so that propagating states from the ferromagnet decay into the tunnel barrier with the symmetry of the ferromagnet/Al_2O_3 contact. Recently, evidence for crystalline growth of α-Al_2O_3 on silicon has been reported.[30] However, the Al_2O_3 has hexagonal structure. Thus any in-plane anisotropy, if it exists, would not have the fourfold symmetry that we observe. More importantly, it is known that the Al_2O_3 and ferromagnet in our devices are, respectively, amorphous and polycrystalline.[23,24] Therefore, we do not expect any kind of anisotropy arising from the crystallinity of the Al_2O_3/ferromagnet contact.

(b) An anisotropy of the spin-relaxation time (τ_s) in silicon will lead to an anisotropic spin accumulation. We discuss the possible mechanisms that may produce an anisotropy in the spin-relaxation time and hence in spin accumulation. In bulk and unstrained silicon the spin-relaxation time is expected to be isotropic.[31] The Dresselhaus type of spin-orbit coupling fields are absent for silicon due to its bulk inversion symmetry. However, due to symmetry breaking at the silicon interface, a contribution from Dresselhaus spin-orbit coupling can be present. This would produce an anisotropy in the spin-relaxation time with fourfold as well as twofold symmetry (see Fig. 4 of Ref. 27). Then, a twofold and fourfold anisotropy would be produced in the spin accumulation in the silicon. However, we observe only a fourfold anisotropy in the measured voltage, implying that this mechanism is absent.

Heterostructures such as Si/oxide/ferromagnet have a built-in potential gradient in the growth direction and hence an electric field perpendicular to the tunnel interfaces. This leads to an effective Rashba spin-orbit coupling field.[27] However, the magnitude of the Rashba field is isotropic within the plane of the interface, and will thus not generate an in-plane tunneling anisotropy.

TABLE I. Summary of the in-plane anisotropy data obtained at −172 mV on tunnel contacts to p-Si and n-Si. Here $R_{\rm tun}$ is the tunnel resistance, $\Delta R_{\rm spin}$ is the spin resistance, and $\Delta R_{\rm in}$ is the maximum peak-to-peak signal for in-plane rotation of the magnetization.

Parameters Units	$\Delta R_{\rm in}$ (Ω)	$R_{\rm tun}$ (Ω)	$\Delta R_{\rm in}/R_{\rm tun}$ (%)	$\Delta R_{\rm spin}$ (Ω)	$\Delta R_{\rm in}/\Delta R_{\rm spin}$ (%)
Crystalline MgO					
p-Si/MgO/Fe	0.976	1865	0.052	22.22	4.39
Polycrystalline MgO					
p-Si/MgO/Fe	0.077	295	0.026	2.44	3.15
Amorphous Al_2O_3					
p-Si/Al_2O_3/Fe	0.265	1811	0.015	14.72	1.8
p-Si/Al_2O_3/Ni	0.026	895	0.002	3.84	0.68
p-Si/Al_2O_3/NiFe	0.021	358	0.005	4.29	0.49
n-Si/Al_2O_3/Fe	0.006	221	0.003	0.44	1.46

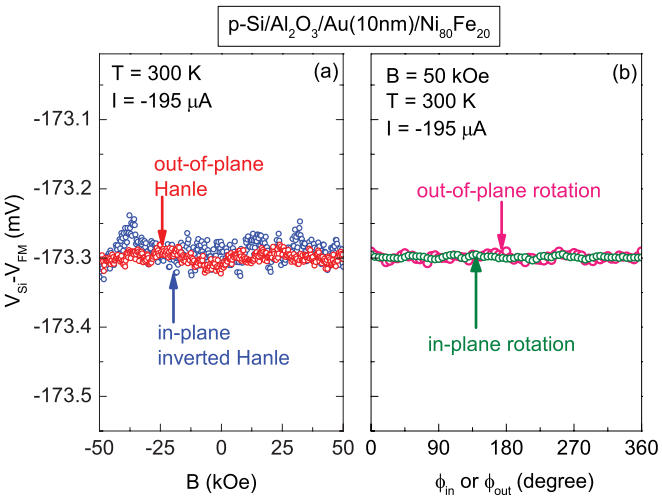

FIG. 12. (Color online) Control experiment with a *p*-type Si device having a nonmagnetic nanolayer (10 nm Au) inserted between the ferromagnetic electrode ($Ni_{80}Fe_{20}$) and the tunnel barrier (Al_2O_3). This suppresses the tunnel spin polarization to zero. (a) Hanle (red) and inverted Hanle (blue) measurements yield a null result. (b) Similarly, a null result is obtained when the magnetization is rotated from in plane to out of plane or within the plane of the magnetic layer (right panel).

(c) Given that the previous two mechanisms are not the source of the in-plane anisotropy, we attribute the anisotropy to a different mechanism that can arise if the tunneling process is coherent. In that case, the propagating states from the ferromagnet couple directly to empty states in the Si. The tunneling states thereby "inherit" part of the character and crystal symmetry of the Si electrode, which is a crystalline wafer with (001) orientation. Together with spin-orbit interaction at the ferromagnet/oxide interface, this may produce an in-plane cubic anisotropy of the tunneling spin polarization, and thereby of the spin accumulation. We suggest that this mechanism, that has previously not been considered, can produce a crystal-induced anisotropy in devices in which only the nonmagnetic electrode (silicon) is crystalline, but the tunnel oxide and ferromagnet are not.

Thus we conclude that the observed *in-plane* anisotropy in devices with an amorphous Al_2O_3 barrier is due to a contribution from coherent spin-polarized transport across the tunnel device and reflects the cubic structure of the crystalline silicon electrode.

C. Control device

In spin-transport measurements on semiconductor-based magnetic tunnel devices, it is important to rule out any source of spurious signals that may interfere with the spin signal.

A suitable control experiment was introduced[6,32] that can be used to prove or disprove spin transport across semiconductor/oxide/ferromagnet tunnel devices. It exploits the extreme interface sensitivity of the spin-polarized tunneling. A nonmagnetic nanolayer inserted between a ferromagnet and a tunnel barrier suppresses the tunnel spin polarization of the magnetic tunnel contact to a negligible value. In such a control device, the true spin-related effects (including the anisotropy) disappear. However, the ferromagnetic materials and any associated spurious effects would still be present.[32] We studied a control sample with structure *p*-type $Si/Al_2O_3/Au(10\ nm)/Ni_{80}Fe_{20}$. It contains a nonmagnetic nanolayer (10 nm of Au) in between the ferromagnet and the tunnel barrier. Figure 12(a) displays the Hanle and inverted Hanle measurements on this device at a bias current of $-195\ \mu A$. The absence of Hanle and inverted Hanle signals [Fig. 12(a)] and of any tunneling anisotropy (*in plane* or *out of plane* [Fig. 12(b)]) shows that signals obtained on the tunnel devices without a nonmagnetic layer are due to spin-polarized transport across the tunnel contact. Therefore, the observed anisotropy is genuine and due to anisotropy of the spin accumulation in the Si.

IV. SUMMARY

We have investigated the crystal-structure dependent anisotropy of spin accumulation in Si/MgO/Fe and Si/Al_2O_3/ferromagnet tunnel devices. The *in-plane* tunneling anisotropy in Si/oxide/ferromagnet tunnel devices displays a fourfold symmetry that reflects the crystal structure of the Si and/or MgO/Fe tunnel contact. The presence of fourfold *in-plane* anisotropy in devices with an amorphous Al_2O_3 barrier indicates a new mechanism of tunneling anisotropy. It arises from the direct coupling of states from the ferromagnet to states in the crystalline Si, as in coherent tunneling, which results in an anisotropy that reflects the cubic structure of the silicon.

ACKNOWLEDGMENTS

This work was financially supported by the Netherlands Foundation for Fundamental Research on Matter (FOM). One of the authors (A.S.) acknowledges a JSPS Postdoctoral Fellowship for Foreign Researchers.

[1] I. Žutić, J. Fabian, and S. Das Sarma, Rev. Mod. Phys. **76**, 323 (2004).
[2] J. Fabian, A. Matos-Abiague, C. Ertler, P. Stano, and I. Žutić, Acta Phys. Slov. **57**, 565 (2007).
[3] D. D. Awschalom and M. E. Flatte, Nature Phys. **3**, 153 (2007).
[4] R. Jansen, Nat. Mater. **11**, 400 (2012).
[5] R. Jansen, S. P. Dash, S. Sharma, and B. C. Min, Semicond. Sci. Technol. **27**, 083001 (2012).
[6] S. P. Dash, S. Sharma, R. S. Patel, M. P. de Jong, and R. Jansen, Nature (London) **462**, 491 (2009).
[7] T. Suzuki, T. Sasaki, T. Oikawa, M. Shiraishi, Y. Suzuki, and K. Noguchi, Appl. Phys. Express **4**, 023003 (2011).
[8] K. R. Jeon, B.-C. Min, Y.-H. Jo, H.-S. Lee, I.-J. Shin, C.-Y. Park, S.-Y. Park, and S.-C. Shin, Phys. Rev. B **84**, 165315 (2011).
[9] H. Saito, S. Watanabe, Y. Mineno, S. Sharma, R. Jansen, S. Yuasa, and K. Ando, Solid State Commun. **151**, 1159 (2011).

[10]S. Iba, H. Saito, A. Spiesser, S. Watanabe, R. Jansen, S. Yuasa, and K. Ando, Appl. Phys. Express **5**, 023003 (2012).
[11]A. Jain, L. Louahadj, J. Peiro, J. C. L. Breton, C. Vergnaud, A. Barski, C. Beigné, L. Notin, A. Marty, V. Baltz, S. Auffret, E. Augendre, H. Jaffrès, J. M. George, and M. Jamet, Appl. Phys. Lett. **99**, 162102 (2011).
[12]C. Li, O. van 't Erve, and B. Jonker, Nat. Commun. **2**, 245 (2011).
[13]T. Sasaki, T. Oikawa, T. Suzuki, M. Shiraishi, Y. Suzuki, and K. Tagami, Appl. Phys. Express **2**, 053003 (2009).
[14]K. R. Jeon, B. C. Min, I. J. Shin, C. Y. Park, H. S. Lee, Y. H. Jo, and S. C. Shin, New J. Phys. **14**, 023014 (2012).
[15]A. Spiesser, S. Sharma, H. Saito, R. Jansen, S. Yuasa, and K. Ando, Proc. SPIE **8461**, 84610K (2012).
[16]W. H. Butler, X.-G. Zhang, T. C. Schulthess, and J. M. MacLaren, Phys. Rev. B **63**, 054416 (2001).
[17]J. Mathon and A. Umerski, Phys. Rev. B **63**, 220403 (2001).
[18]S. Yuasa, T. Nagahama, A. Fukushima, Y. Suzuki, and K. Ando, Nat. Mater. **3**, 868 (2004).
[19]S. S. P. Parkin, C. Kaiser, A. Panchula, P. M. Rice, B. Hughes, M. Samant, and S.-H. Yang, Nat. Mater. **3**, 862 (2004).
[20]M. Ciorga, A. Einwanger, U. Wurstbauer, D. Schuh, W. Wegscheider, and D. Weiss, Physica E **42**, 2673 (2010).
[21]S. Sharma, S. P. Dash, H. Saito, S. Yuasa, B. J. van Wees, and R. Jansen, Phys. Rev. B **86**, 165308 (2012).
[22]S. P. Dash, S. Sharma, J. C. Le Breton, J. Peiro, H. Jaffrès, J. M. George, A. Lemaitre, and R. Jansen, Phys. Rev. B **84**, 054410 (2011).
[23]B. C. Min, K. Motohashi, C. Lodder, and R. Jansen, Nat. Mater. **5**, 817 (2006).
[24]B. C. Min, Ph.D. thesis, Koninklijke Wöhrmann, Zutphen, The Netherlands, 2007 .
[25]C. Gould, C. Rüster, T. Jungwirth, E. Girgis, G. M. Schott, R. Giraud, K. Brunner, G. Schmidt, and L. W. Molenkamp, Phys. Rev. Lett. **93**, 117203 (2004).
[26]H. Saito, S. Yuasa, and K. Ando, Phys. Rev. Lett. **95**, 086604 (2005).
[27]A. Matos-Abiague and J. Fabian, Phys. Rev. B **79**, 155303 (2009).
[28]S. P. Dash, S. Sharma, J. C. L. Breton, and R. Jansen, Proc. SPIE **7760**, 77600J (2010).
[29]In principle, the prefactor in the last term should include A_1 and A_2. However, during fitting we observed that inclusion of these terms does not affect the previously extracted value of A_1 and A_2. Retaining ΔR_{spin} as a prefactor makes the fitting procedure simple.
[30]T. Inokuchi, M. Ishikawa, H. Sugiyama, Y. Saito, and N. Tezuka, J. Appl. Phys. **111**, 07C316 (2012).
[31]Y. Song and H. Dery, Phys. Rev. B **86**, 085201 (2012).
[32]R. S. Patel, S. P. Dash, M. P. de Jong, and R. Jansen, J. Appl. Phys. **106**, 016107 (2009).